10902 *Biochemistry* **2010,** *49,* 10902–10911
DOI: 10.1021/bi101562m

BIOCHEMISTRY
including biophysical chemistry & molecular biology
Article

Detection of Organometallic and Radical Intermediates in the Catalytic Mechanism of Methyl-Coenzyme M Reductase Using the Natural Substrate Methyl-Coenzyme M and a Coenzyme B Substrate Analogue[†]

Mishtu Dey,[‡] Xianghui Li,[§] Ryan C. Kunz,[∥] and Stephen W. Ragsdale*

Department of Biological Chemistry, University of Michigan, Ann Arbor, Michigan 48109, United States.
[‡]*Current address: Department of Chemistry, Massachusetts Institute of Technology, Cambridge, Massachusetts 02139.* [§]*Current address: New England Biolabs, Inc., Shanghai R&D Center, Shanghai, China.*
[∥]*Current address: Department of Cell Biology, Harvard Medical School, Boston, Massachusetts 02115*

Received September 26, 2010; Revised Manuscript Received November 15, 2010

ABSTRACT: Methyl-coenzyme M reductase (MCR) from methanogenic archaea catalyzes the terminal step in methanogenesis using coenzyme B (CoBSH) as the two-electron donor to reduce methyl-coenzyme M (methyl-SCoM) to form methane and the heterodisulfide, CoBS-SCoM. The active site of MCR contains an essential redox-active nickel tetrapyrrole cofactor, coenzyme F_{430}, which is active in the Ni(I) state (MCR_{red1}). Several catalytic mechanisms have been proposed for methane synthesis that mainly differ in whether an organometallic methyl-Ni(III) or a methyl radical is the first catalytic intermediate. A mechanism was recently proposed in which methyl-Ni(III) undergoes homolysis to generate a methyl radical (Li, X., Telser, J., Kunz, R. C., Hoffman, B. M., Gerfen, G., and Ragsdale, S. W. (2010) *Biochemistry 49*, 6866−6876). Discrimination among these mechanisms requires identification of the proposed intermediates, none of which have been observed with native substrates. Apparently, intermediates form and decay too rapidly to accumulate to detectible amounts during the reaction between methyl-SCoM and CoBSH. Here, we describe the reaction of methyl-SCoM with a substrate analogue (CoB_6SH) in which the seven-carbon heptanoyl moiety of CoBSH has been replaced with a hexanoyl group. When MCR_{red1} is reacted with methyl-SCoM and CoB_6SH, methanogenesis occurs 1000-fold more slowly than with CoBSH. By transient kinetic methods, we observe decay of the active Ni(I) state coupled to formation and subsequent decay of alkyl-Ni(III) and organic radical intermediates at catalytically competent rates. The kinetic data also revealed substrate-triggered conformational changes in active Ni(I)-MCR_{red1}. Electron paramagnetic resonance (EPR) studies coupled with isotope labeling experiments demonstrate that the radical intermediate is not tyrosine-based. These observations provide support for a mechanism for MCR that involves methyl-Ni(III) and an organic radical as catalytic intermediates. Thus, the present study provides important mechanistic insights into the mechanism of this key enzyme that is central to biological methane formation.

Methane is a carbon and energy source for methanotrophic microbes and an important source of renewable energy for humans; on the other hand, it is the most abundant hydrocarbon in the atmosphere and is a potent greenhouse gas. Methanogens are responsible for the production of more than 90% of the earth's atmospheric methane (*1*). Methyl-coenzyme M reductase (MCR)[1] from methanogenic archaea catalyzes the rate-limiting and terminal step in the biological synthesis of methane, the process by which methanogenic archaea conserve energy (*2*, *3*), and the first step in anaerobic methane oxidation (*4*−*8*). With the use of coenzyme B (CoBSH) as a two-electron donor, MCR reduces methyl-coenzyme M (methyl-SCoM) to methane and the mixed disulfide product, CoBS-SCoM (*9*, *10*). This reaction is responsible for the annual generation of approximately 1 billion tons of methane. The active site of MCR contains a redox-active Ni-tetrapyrrolic cofactor called Coenzyme F_{430} (*11*, *12*) that is thought to play an essential role in catalysis and is active in the Ni(I) state (*13*, *14*). The role of nickel in the MCR catalytic cycle is controversial and four competing mechanisms have been proposed, with the two limiting mechanisms presented in Figure 1.

As proposed in Mechanism I (*15*−*17*), which is based on studies with F_{430} model complexes and on the location of substrates (and analogues) in the active site cavity in the crystal structures of the inactive Ni(II) enzyme, a nucleophilic attack of Ni(I) on the methyl group of methyl-SCoM takes place in the first step, generating a methyl-Ni(III) intermediate and releasing the $^{-}$SCoM thiolate anion. Next, $^{-}$SCoM transfers one electron to methyl-Ni(III) to generate an $^{\bullet}$SCoM thiyl radical and a methyl-

[†]This work was supported by the DOE (Grant ER15931 to S.W.R.).
*To whom correspondence should be addressed. Stephen W. Ragsdale, Department of Biological Chemistry, University of Michigan Medical School, 1150 W. Medical Center Dr., Ann Arbor, MI 48109-0606. Telephone: 734-615-4621. Fax: 734-763-4581. E-mail: sragsdal@umich.edu.

[1]Abbreviations: MCR, methyl-coenzyme M reductase; methyl-SCoM, methyl-coenzyme M; CoB_6SH, *N*-6-mercaptohexanolyl-threonine phosphate; CoB_5SH, *N*-5-mercaptopentanolyl-threonine phosphate; HSCoM, Coenzyme M; CoBSH, *N*-7-mercaptoheptanolyl-threonine phosphate; BES, 2-bromoethanesulfonate; CoBS-SCoM, the heterodisulfide product of the MCR reaction; EPR, electron paramagnetic resonance.[2] Surprisingly, these values for the transient kinetic experiment are approximately 10-fold lower than the steady state k_{cat}/K_M value for methane formation from methyl-SCoM and CoB_6SH (1.0×10^5 M^{-1} s^{-1} at 20 °C and 1.6×10^6 M^{-1} s^{-1} at 65 °C). The issue appears to relate to the value of K_M, which we find to be ~50-fold higher than the values determined previously (*28*).

 Published on Web 11/22/2010

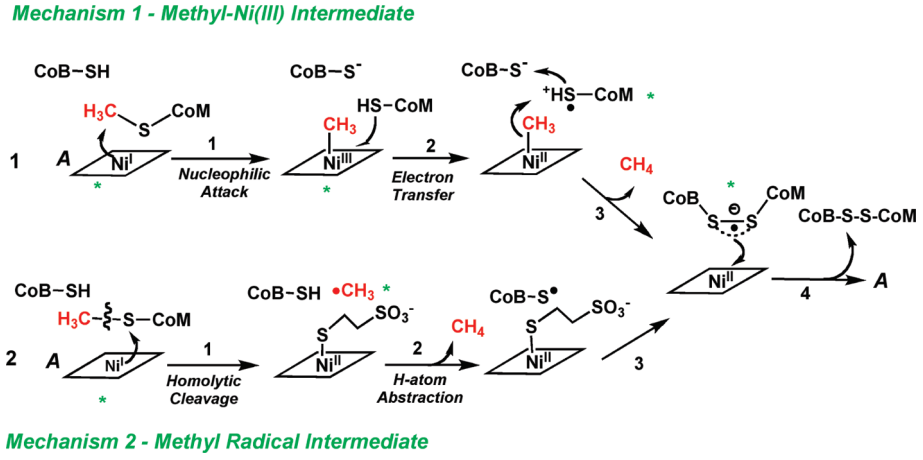

FIGURE 1: Competing mechanisms for methane formation by MCR. The asterisks (*) designate species that should give rise to EPR spectra.

Ni(II) species, which undergoes protonolysis to form methane and the Ni(II) state of F_{430}. Then, the SCoM thiyl radical is proposed to react with the thiolate of CoBSH to form a disulfide anion radical, which is sufficiently reducing to convert Ni(II) back to the active Ni(I) state (the $E°$ of the Ni(II)/(I) couple is below −600 mV versus NHE (normal hydrogen electrode)) (*18*, *19*) and thus complete the catalytic cycle. Mechanism II (*20*−*22*), which is based on density function theory calculations, considers the methyl-Ni(III) species proposed in Mechanism I to be an ineffectual intermediate. This is because the difference in bond energy between the relatively strong methyl-S bond of methyl-SCoM and the relatively weak methyl-Ni(III) would require the first step of the reaction to be endothermic with an activation enthalpy of ~55 kcal/mol. Therefore, as proposed in Mechanism II (Figure 1, bottom), Ni(I) reacts with the sulfur atom adjacent to the methyl group of methyl-SCoM, promoting the homolytic cleavage of the methyl-sulfur bond and generating a methyl radical and a Ni(II)-thiolate complex. The methyl radical is proposed to abstract a hydrogen atom from CoBSH to generate a CoBS thiyl radical that reacts with bound HSCoM to form a disulfide anion radical and Ni(II). Finally, reduction of Ni(II) to active Ni(I) and generation of the heterodisulfide product takes place as in Mechanism I. In Mechanism III, which is also based on density functional theory computations, protonation of Coenzyme F_{430} (*23*) is proposed to promote reductive cleavage of the methyl-SCoM thioether bond to generate a nickel center that is coordinated by $^{-}CH_3$ and $^{-}$SCoM anions and two of the tetrapyrrole nitrogens. The $CoBS^{-}$ anion is then proposed to react with $^{-}$SCoM to form the heterodisulfide product and methyl-Ni(III). Formation of methane requires the proton that was initially donated to coenzyme F_{430}. Mechanism IV, based on transient kinetic studies with bromoethanesulfonate (BES) and CoB_6SH, proposes a hybrid mechanism that includes both methyl-Ni and methyl radical intermediates. As in Mechanism I, Mechanism IV invokes nucleophilic attack of Ni(I) on methyl-SCoM to generate methyl-Ni(III), which undergoes homolysis to form a methyl radical and Ni(II) (*24*). The methyl radical is proposed to abstract a hydrogen atom from a nearby species to generate a more stable radical; finally subsequent steps are similar to those proposed in Mechanisms I and II. Which of the four mechanisms is correct could be determined by trapping and characterizing the intermediates formed during the initial steps of catalysis, i.e., whether they involve an organometallic methyl-Ni(III) intermediate and/or a methyl radical and a Ni(II)-thiolate complex. So far, in studies with the natural substrates (methyl-SCoM and CoBSH), none of the proposed intermediates in the two mechanisms have been identified, presumably because they do not accumulate, decaying too rapidly to be observed by stopped-flow and rapid freeze-quench EPR methods. Thus, upon reaction of MCR_{red1} with methyl-SCoM, the EPR spectrum of Ni(I)-MCR_{red1} remains and no other detectible intermediates are observed.

An intermediate does not accumulate because its formation rate is too slow relative to the rate of decay. Thus, in order to trap a catalytic intermediate in the MCR mechanism, two possible approaches have been considered: to accelerate the first step or to slow down subsequent steps of catalysis. The first approach, acceleration of the first step of the reaction, was recently demonstrated using several classes of alkyl halides, which are highly activated methyl (or alkyl) donating methyl-SCoM substrate analogues (*25*−*28*). Ni(I)-MCR_{red1} reacts with various alkyl halides to generate the corresponding alkyl-Ni(III) species at rates exceeding the rate of methane formation using natural substrates. A broad range of haloalkanoates and haloalkane sulfonates could be used, indicating a fair degree of flexibility within the active site of MCR. Smaller halogenated substrates appear to occupy the methyl-SCoM binding site, while the longer chain substrates occupy the position of HSCoB in the substrate channel leading from the surface toward cofactor F_{430} (*25*). The alkyl-Ni(III) species were subject to protonolysis to generate the corresponding alkane (*26*, *28*). Surprisingly, reaction of the alkyl-Ni(III) complexes (produced by reacting MCR_{red1} with haloalkanes) with thiolates, resulted in generation of the active Ni(I)-MCR_{red1} state and the corresponding thioether products, i.e., methyl-SCoM when methyl-Ni(III) is reacted with HSCoM (*27*). These experiments support the intermediacy of an alkyl-nickel intermediate in methanogenesis because they demonstrate that formation of the alkyl-Ni(III) species can be coupled to alkane formation by protonolysis, similar to the methanogenesis reaction, or to thioether formation, which mimics the reverse reaction of methane conversion to methyl-SCoM. The catalytic competence of the methyl-Ni(III) species is also supported by the demonstration that this species reacts with HSCoM and CoBSH to generate methane with a rate constant (k_{obs} = 1.1 s^{-1} at 25 °C) that is similar to the steady-state turnover number (k_{cat}) for methane formation from the natural substrates (4.5 s^{-1} at 25 °C) (*29*). Thus, the first approach of accelerating the first step of catalysis provides support for the catalytic relevance of the methyl-Ni(III)

intermediate in methane formation by MCR. However, an inherent limitation to the use of bromoalkane substrate analogues is that it involves the use of highly activated alkyl donors, not the natural methyl donor (methyl-SCoM).

The goal of the present study was to trap intermediates in the MCR mechanism by using the second approach described above (i.e., decelerating subsequent steps) by incubating MCR_{red1} with the natural substrate methyl-SCoM and a substrate analogue of CoBSH that is either one or two methylene group shorter than CoBSH (i.e., CoB_6SH and CoB_5SH) and serves as a slow substrate in steady-state and single turnover reactions (*10*, *30*). On the basis of the structure of CoBSH within the substrate channel above the F_{430} cofactor, the hypothesis driving the studies described in this paper is that the reactive thiolate of CoB_6SH and CoB_5SH would be located ~2.0−3.0 Å more distant from the first intermediate (i.e., methyl-Ni or methyl radical) and would, thus, react slower than CoBSH, perhaps leading to the accumulation of (and allowing the observation of) the first intermediate in the reaction. CoB_6SH was surmised to be an obvious choice for this purpose since it binds tightly to MCR ($K_M = 0.1\ \mu M$ (*10*)) and serves as a substrate with methyl-SCoM as the methyl donor, leading to a 100- (*10*) to 1000-fold (*30*) reduction (relative to CoBSH) in the k_{cat} for methane formation under steady-state conditions and a 440-fold reduction in methane synthesis under single turnover conditions (*30*).

Here, we demonstrate that a transient alkyl-Ni(III) and an organic radical intermediates are generated from the reaction of MCR_{red1} with CoB_6SH and methyl-SCoM and that the radical forms and decays at a rate consistent with its intermediacy in methanogenesis. On the basis of the structure of the Ni(II) form of MCR with the phenol(ate) oxygens of two tyrosine residues (αTyr333 and βTyr367) located directly above the upper axial Ni ligand (*31*), it seemed likely that the radical would be a Tyr radical. However, EPR spectroscopic studies coupled with isotope labeling experiments rule out the possibility that the organic radical is a tyrosyl radical; instead, the radical has properties suggestive of a sulfur-based thiyl radical. We propose a mechanism that, like Mechanism I, involves a methyl-Ni(III) intermediate that undergoes reduction to a Ni(II)-MCR species. Subsequent electron and proton transfer from a nearby moeity (perhaps HSCoM, CoBSH, thioglycine, Tyr) forms methane and the newly identified radical. We clearly demonstrate that the relatively stable radical identified here is not a tyrosyl radical and we speculate that the observed radical intermediate identified here may be CoMS- or CoBS-based. Decay of this radical would then be coupled to the final steps of methanogenesis in which the active MCR_{red1} state is regenerated.

MATERIALS AND METHODS

Materials and Organism. Methanothermobacter marburgensis was obtained from the Oregon Collection of Methanogens (Portland, OR) catalog as OCM82. All buffers, media ingredients, and other reagents were acquired from Sigma-Aldrich (St. Louis, MO) and, unless otherwise stated, were of the highest purity available. Solutions were prepared using Nanopure deionized water. N_2 (99.98%), H_2/CO_2 (80%/20%), and Ultra High Purity (UHP) H_2 (99.999%) were obtained from Cryogenic Gases (Grand Rapids, MI). Ti(III) citrate solutions were prepared from a stock solution of 200 mM Ti(III) citrate, which was synthesized by adding sodium citrate to Ti(III) trichloride (30 wt % solution in 2 N hydrochloric acid) (Acros Organics, Morris Plains, NJ) under anaerobic conditions and adjusting the pH to 7.0 with sodium bicarbonate (*32*). The concentration of Ti(III) citrate was determined routinely by titrating a methyl viologen solution.

Synthesis of Methyl-SCoM, CoB_5SH, CoB_6SH, CoB_7SH, CoB_8SH, and [$^2H_6$]-p-OH-Phenylacetic Acid. Methyl-SCoM was prepared from HSCoM and methyl iodide (*33*). The homodisulfides, CoB_nS-$SCoB_n$ (n = 5−9), were prepared as described from the corresponding bromoacids, e.g., 5-bromovaleric acid for CoB_5SH (Sigma-Aldrich, St. Louis, MO) (*34*). The free thiol forms of CoB_nSH were generated by reduction of the homodisulfides as previously described (*27*). [$^2H_6$]-*p*-OH-phenylacetic acid was synthesized from *p*-OH phenylacetic acid using [$^2H_4$]-acetic acid and DCl in D_2O. Specifically, 200 mg of *p*-hydroxyphenylacetic acid was dissolved in 1.2 mL of [$^2H_4$] acetic acid and 3.2 mL of 20% DCl in D_2O, and the reaction was performed in a sealed tube for 5 h at 190 °C as described previously (*35*). The yield was measured by mass spectrometry with the following distribution of deuterium: 80% of [$^2H_6$]-, 18% of [$^2H_5$]-, and 2% of [$^2H_4$]-*p*-hydroxyphenylacetic acid.

M. marburgensis Growth and Harvest and MCR_{red1} Purification. Solutions were prepared and all manipulations were performed under strictly anaerobic conditions in a Vacuum Atmospheres (Hawthorne, CA) anaerobic chamber maintained under nitrogen gas at < 1 ppm of oxygen. MCR_{red1} was isolated from *M. marburgensis* cultured on H_2/CO_2 (80%/20%) at 65 °C in a 14 L fermentor (New Brunswick Scientific Co., Inc. New Brunswick, NJ). Culture media were prepared as previously described (*28*) with a slight modification of the sulfur and reducing source. Instead of H_2S used previously, 50 mM sodium sulfide was added at a flow rate of 1 mL/min during the entire growth period. MCR_{red1} was generated *in vivo* and purified as described earlier (*28*). This purification procedure routinely generates about 70% MCR_{red1} as determined by UV−visible (see the starting spectrum in Figure 2 as representative) and EPR spectroscopies (*28*).

To generate samples of MCR that contained a tyrosine isotopologue ($^2H_6$-Tyr), feeding experiments were performed in which *M. marburgensis* cultures were grown with 0.1 mM phenyl acetate, 0.2 mM [$^2H_6$]-*p*-hydroxyphenylacetate, and 0.02 mM indoleacetate. The $^2H_6$-Tyr- labeled MCR_{red1} was isolated and subjected to peptide hydrolysis followed by mass spectrometric analysis. Additionally, amino acid analyses were used to determine the amount of [$^2H_6$]-*p*-hydroxyphenylacetic acid incorporated into the tyrosine residues in MCR, as previously described (*24*). The results showed that at least 50% of tyrosine residues in MCR were labeled with $^2H_4$-Tyr instead of $^2H_6$-Tyr. This is a lower estimate of the labeling percentage because significant H-exchange occurs during the acid hydrolysis. A similar estimate of the labeling percentage was obtained by mass spectrometric analysis of BrCN- and AspN-digested fragments of MCR isolated from cells grown on labeled hydroxyphenylacetate, e.g., greater than 50% of βTyr367 was labeled. Even though the fragment including αTyr333 was not identified, 11 other peptides containing tyrosine residues showed a similar percentage of $^2H_6$-Tyr labeling. Thus, independent amino acid and peptide analyses confirmed that the Tyr residues in MCR were significantly labeled when cells were fed with $^2H_6$-hydroxyphenylacetate under the conditions described.

O-Acetylation of tyrosine in MCR was obtained through treatment of 130 μM MCR with 280 mM *N*-acetylimidazole on

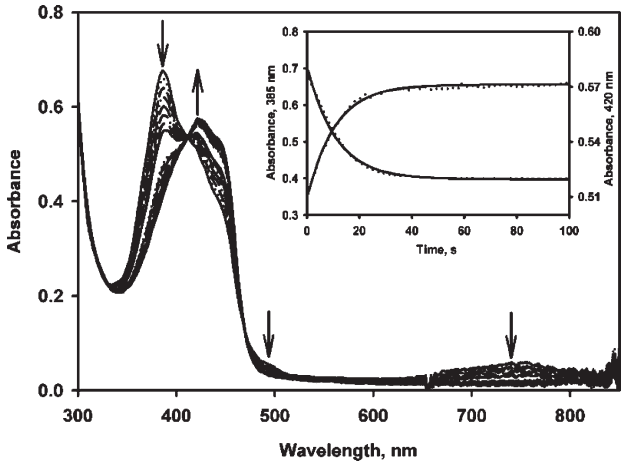

FIGURE 2: UV−visible spectral changes when MCR_{red1} is incubated with CoB_6SH and methyl-SCoM. MCR_{red1} (30 μM) was reacted with 60 μM CoB_6SH and 1 mM methyl-SCoM in 50 mM Tris-HCl, pH 7.6, at 25 °C. Arrows indicate the direction of change over time. Inset: Time-dependent UV−visible changes when MCR_{red1} is reacted with CoB_6SH and methyl-SCoM. The data were fit to single exponential equations [$f = y_0 + a\exp(-bx)$ and $f = y_0 + a(1 - \exp(-bx))$] with $k_{385} = 0.091 \pm 0.001\ s^{-1}$; $k_{420} = 0.095 \pm 0.002\ s^{-1}$.

ice for 2.5 h. The excess *N*-acetylimidazole was removed with a 30 kDa molecular mass cutoff filter.

Spectroscopy of MCR. UV−visible spectra of MCR were recorded in the anaerobic chamber using a diode array spectrophotometer (model DT 1000A, Analytical Instrument Systems, Inc., Flemington, NJ). X-band EPR spectra were recorded on a Bruker EMX spectrometer (Bruker Biospin Corp., Billerica, MA), equipped with an Oxford ITC4 temperature controller, a Hewlett-Packard model 5340 automatic frequency counter, and Bruker gaussmeter. Unless otherwise noted, the EPR spectroscopic parameters included temperature, 70 K; microwave power, 10 mW; microwave frequency, 9.43 GHz; receiver gain, 2×10^4; modulation amplitude, 10.0 G; modulation frequency, 100 kHz. Double integrations of the EPR spectra were performed and referenced to a 1 mM copper perchlorate standard. NMR spectra were acquired at 298 K on a Bruker Avance DRX 500 MHz instrument equipped with a TXI cryoprobe.

Stopped-Flow Studies. Stopped-flow experiments were performed using an Applied Photophysics (Leatherhead, U.K.) spectrophotometer (SX.MV18 with the Pro-Data upgrade) equipped with a photodiode array detector. The sample handing unit (drive syringes and mixing chamber) of the stopped-flow is housed in a Vacuum Atmospheres anaerobic chamber maintained at an oxygen tension below 1 ppm. In addition, rigorous measures were taken to remove any trace oxygen by flushing the drive syringes and mixing chamber with a dithionite/resazurin (1 mM:0.02 mM) solution in 0.1 M NaOH. MCR_{red1} was incubated with the first substrate (CoB_6SH or methyl-SCoM) and rapidly mixed with varied concentrations of the second substrate at 25 °C. The reaction was monitored in the single wavelength mode by following the decay of MCR_{red1} at 385 nm or the formation of the Ni(II) or Ni(III) states of MCR at 420 nm, using a 1 cm path length cell. Data were fit to single exponential decay functions at high concentrations and double exponential functions at low concentrations using the Pro-Data software provided by Applied Photophysics. Reported rate constants are the average of at least three different rapid-mixing experiments.

Data Analysis and Equations. Data were fit with either Pro-Data software from Applied Photophysics or Sigma Plot (Systat Software Inc., Point Richmond, CA). Radical formation and/or decay in Figure 4 were fit to a sequential two-step nonreversible reaction (A → B → C). The data for [A] were fit to eq 1

$$[A] = [A]_0\, e^{-kt} \quad (1)$$

using Sigma Plot, where [A] and $[A]_0$ are the time-dependent and initial intensities of the MCR_{red1} EPR signal, t is time, and k is the first-order rate constant for MCR_{red1} decay. The data for [B] were fit to eq 2 using Sigma Plot

$$[B] = ([A]_0\{k_1/(k_2 - k_1)\})(e^{-k_1 t} - e^{-k_2 t}) \quad (2)$$

where [B] is the EPR intensity of the organic radical signal centered at 3330 G, $[A]_0$ is the initial MCR_{red1} EPR signal, t is time, k_1 is the first-order rate constant for radical formation, and k_2 is the first-order rate constant for radical decay.

RESULTS

UV−Visible Characterization of the Reaction of MCR_{red1} with Methyl-SCoM and Analogues of CoBSH. When MCR_{red1} reacts with methyl-SCoM and CoB_6SH, there is a decrease in the UV−visible bands centered at 385 and 730 nm that are associated with the Ni(I) state of MCR_{red1}, while a peak increases at 420 nm, which is typical of both the Ni(II) and alkyl-Ni(III) states (Figure 2). Additionally, a shoulder centered at 495 nm is observed that decays rapidly. This 495 nm shoulder is a characteristic feature of the alkyl-Ni(III) state of MCR (*25*, *36*, *37*). If MCR_{red1} is incubated with either methyl-SCoM or CoB_6SH alone, no change in the UV−visible spectrum is observed; thus, the reaction is dependent on the presence of both substrates. This observation is consistent with previous studies indicating that the mechanism of MCR proceeds *via* a ternary complex (*10*, *30*, *38*, *39*).

The rate constant of MCR_{red1} decay (0.092 s^{-1}) matches that of Ni(III)/Ni(II) formation (0.095 s^{-1}, at 420 nm) (Figure 2, inset), suggesting that no intermediate is formed between the states. Alternatively, any intermediate that forms does not accumulate to detectable levels or an intermediate with an identical absorption at 420 nm (e.g., alkyl-Ni(III) species) is formed. The observed UV−visible change appears to be catalytically relevant since the value of k_{obs} (~0.092 s^{-1} at 28 °C) is significantly faster than the steady state k_{cat} for methane formation from methyl-SCoM and CoB_6SH (0.16 s^{-1} at 65 °C, which is expected to be ~0.018 s^{-1} at 28 °C). Additionally, a shoulder rapidly appears in the 470−520 nm region (centered at 495 nm), which is characteristic of the alkyl-Ni(III) state of MCR and then decays with a rate constant of 0.172 s^{-1} (Figure 3, inset). The shoulder at 495 nm supports a methyl-Ni(III) intermediate instead of other known MCR states (e.g., MCR_{ox1}) (*25*, *36*, *37*). The rate constant of decay of the 495 nm species (0.172 s^{-1}) is faster than that for decay of Ni(I) (~0.092 s^{-1}), indicating that the Me-Ni(III) state of MCR is transiently formed and only accumulates to low levels (Figure 3).

The decay of MCR_{red1} and the formation of the Ni(III)/Ni(II) state are dependent on the concentrations of both CoB_6SH and methyl-SCoM (Figure 4), with a maximum rate constant of 0.9−1.5 s^{-1} at 25 °C, which would correspond to a k_{max} of 14−24 s^{-1} at 65 °C. This k_{max} value is about 120-fold higher than the steady-state k_{cat} for methane formation from methyl-SCoM and CoB_6SH (0.16 s^{-1} at 65 °C) (*29*). The second order rate constants measured from the stopped flow experiment are $1.5 \times 10^4\ M^{-1}\ s^{-1}$ (at 385 nm),

1.1×10^4 M^{-1} s^{-1} (at 420 nm) for methyl-SCoM dependence (Figure 4, left panel) and 7.5×10^3 M^{-1} s^{-1} (at 385 nm), 0.4×10^3 M^{-1} s^{-1} (at 420 nm) for CoB_6SH dependence (Figure 4, right panel). The values are nearly 2−15 times larger than the values of k_{cat}/K_M for methane formation from its natural substrates (930 M^{-1} s^{-1} for methyl-SCoM and 2.2×10^3 M^{-1} s^{-1} for CoBSH, both at 20 °C) (*29*). These results indicate that the species formed from the reaction of MCR_{red1} with methyl-SCoM and CoB_6SH is kinetically competent as a catalytic intermediate(s) in the process of methane formation and that the kinetics of the CoBSH binding step are very similar when CoBSH or CoB_6SH are used as substrates.

The observed UV−visible changes appear to be biphasic at low substrate concentrations (0.02−0.5 mM of the first substrate with a saturated concentration of the second substrate) with MCR_{red1} decay rate constants in the range of $k_1 = 0.20 \pm 0.04$ to 0.84 ± 0.01 s^{-1} (fast phase) and $k_2 = 0.026 \pm 0.003$ to 0.23 ± 0.08 s^{-1} (slow phase) (at 25 °C), which are similar to those for Ni(II)/Ni(III) formation ($k_1 = 0.13 \pm 0.01$ to 0.79 ± 0.02 s^{-1}, $k_2 = 0.023 \pm 0.004$ to 0.21 ± 0.05 s^{-1}) (Figure S1 in the Supporting Information). The biphasic kinetic data at low substrate concentration can be described by the existence of two populations of the enzyme: one that reacts with the substrate and undergoes a conformational change and the other population that leads to unproductive substrate binding. At low substrate concentrations, the active enzyme population that rapidly binds substrate could undergo a substrate-induced conformational change and react with available substrate (represented by the fast phase, k_1 of the biphasic reaction), while the residual enzyme that gradually binds substrate undergoes a slower reaction (slow phase, k_2 of the biphasic reaction). On the other hand, at higher substrate concentrations, both enzyme populations would contain bound substrate (the first substrate) and be well-poised to rapidly react with the second substrate to form the transient alkyl-Ni(III) species and/or Ni(II), thus exhibiting a single rate constant (k of the monophasic reaction). This model explains the convergence of k_2 to the value of k_1 as the concentration of substrate increases and the dependence of the rate constants of both k_1 and k_2 on the concentrations of methyl-SCoM and CoB_6SH (data not shown).

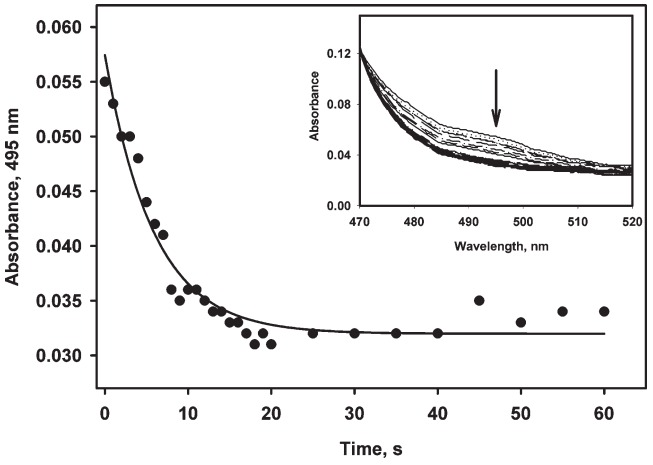

FIGURE 3: Time-dependent decrease in absorbance observed at 495 nm [Ni(III) region] when MCR_{red1} is reacted with CoB_6SH and methyl-SCoM. MCR_{red1} (30 μM) was reacted with 60 μM CoB_6SH and 1 mM methyl-SCoM in 50 mM Tris-HCl, pH 7.6, at 25 °C. Arrow indicates the direction of change over time. Inset: UV−visible spectral changes when MCR_{red1} is incubated with CoB_6SH and methyl-SCoM. The data were fit to single exponential equation [$f = y_0 + a \exp(-bx)$] with $k_{495} = 0.17 \pm 0.02$ s^{-1}.

The substrate-induced conformational change is further supported by the large variation in amplitude of the faster phase of the reaction. As shown in Figure 5, like the rate constant, the amplitude of the fast phase monitored at 385 nm exhibits a hyperbolic dependence on concentrations of both methyl-SCoM and CoB_6SH, yielding K_m values of 0.03 ± 0.02 mM (methyl-SCoM dependence) and 0.08 ± 0.02 mM (CoB_6SH dependence). These values are very similar to those derived from the rate constant (k_{obs}) versus concentration data. The amplitude change at 420 nm is also dependent on the concentrations of both the substrates and yields similar K_M values (Figure S2 in the Supporting Information). Because the amplitudes can be considered to represent relative populations of enzyme that exhibit a particular activity, these data support the hypothesis of two enzyme

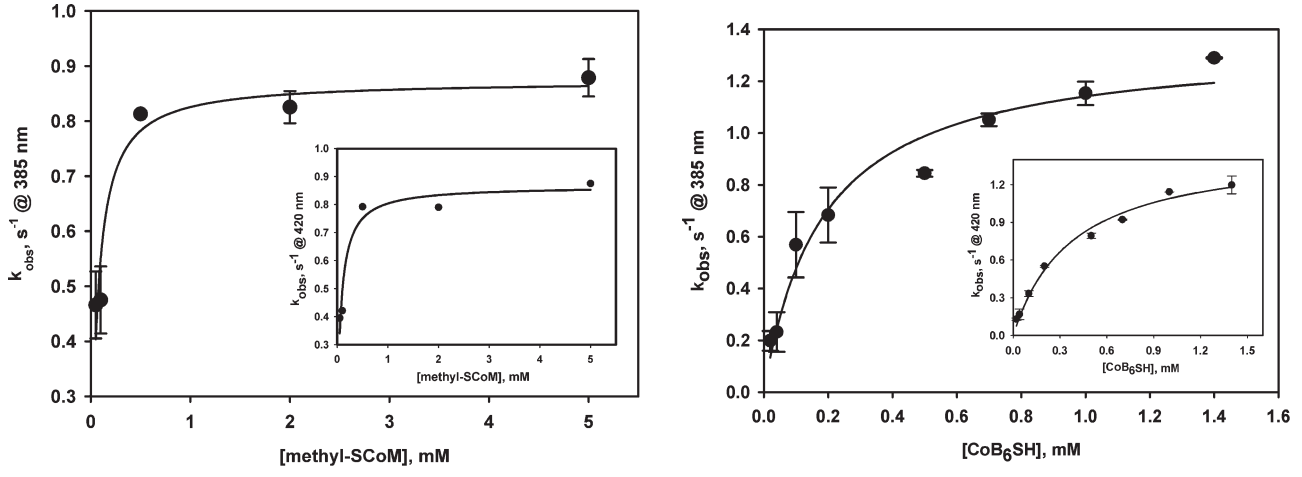

FIGURE 4: Dependence of rate constant (k_{obs}) on substrate concentrations for the reaction of MCR_{red1} with methyl-SCoM and CoB_6SH monitored at 385 and 420 nm. Left panel: MCR_{red1} (10 μM) was reacted with 500 μM CoB_6SH and titrated against various concentrations of methyl-SCoM. At 385 nm: $k_{max} = 0.87 \pm 0.04$ s^{-1}, $K_M = 0.06 \pm 0.01$ mM, $k_{max}/K_M = 1.5 \times 10^4$ M^{-1} s^{-1}. Inset (at 420 nm): $k_{max} = 0.87 \pm 0.08$ s^{-1}, $K_M = 0.08 \pm 0.02$ mM, $k_{max}/K_M = 1.1 \times 10^4$ M^{-1} s^{-1}. The data were fit to a two-parameter hyperbolic equation and the plots were obtained using k_{obs} ("k_1" of biphasic plots at lower substrate concentrations and of "k" at higher concentrations of substrate) determined at 385 and 420 nm. Right panel: MCR_{red1} (10 μM) was reacted with 1 mM methyl-SCoM and varying concentrations of CoB_6SH. At 385 nm: $k_{max} = 1.35 \pm 0.09$ s^{-1}, $K_M = 0.18 \pm 0.04$ mM, $k_{max}/K_M = 7.5 \times 10^3$ M^{-1} s^{-1}. Inset (at 420 nm): $k_{max} = 1.49 \pm 0.09$ s^{-1}, $K_M = 0.37 \pm 0.06$ mM; $k_{max}/K_M = 0.4 \times 10^3$ M^{-1} s^{-1}.

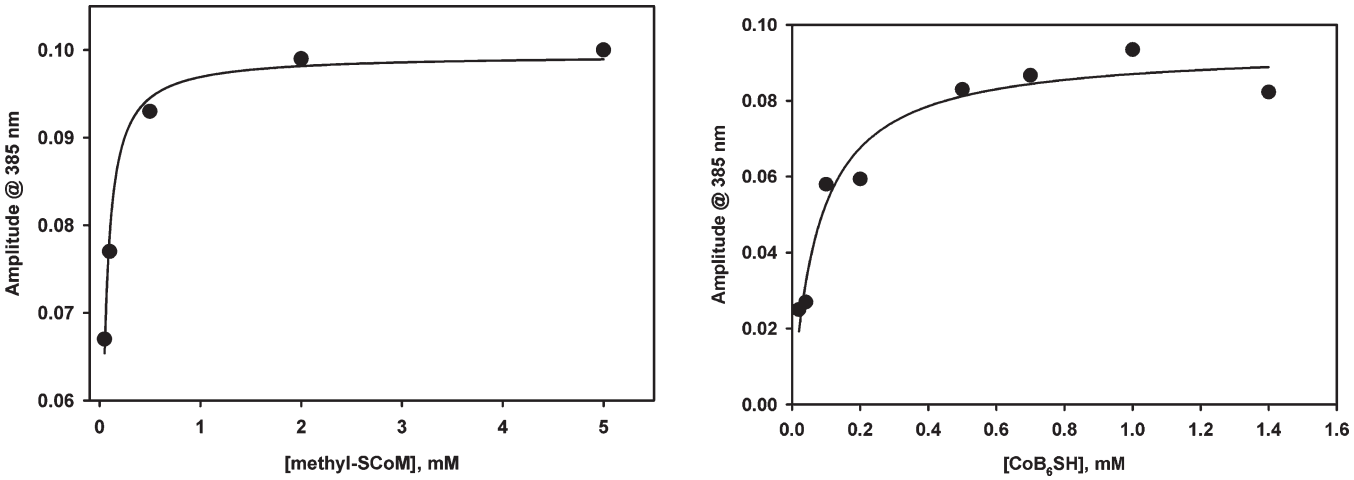

FIGURE 5: Substrate-triggered conformational change of MCR_{red1} upon reaction with methyl-SCoM and CoB_6SH determined by the large-amplitude change as a function of substrate concentrations monitored at 385 nm. Left (varying methyl-SCoM, monitored at 385 nm): amplitude change when MCR_{red1} (10 μM) was treated with saturated CoB_6SH (500 μM) and reacted with different concentrations of methyl-SCoM; $k_{max} = 0.10 \pm 0.01\ s^{-1}$, $K_M = 0.03 \pm 0.02$ mM. Right (varying CoB_6SH, monitored at 385 nm): amplitude change when MCR_{red1} (10 μM) was reacted with 1 mM methyl-SCoM and varying concentrations of CoB_6SH; $k_{max} = 0.09 \pm 0.01\ s^{-1}$, $K_M = 0.08 \pm 0.02$ mM.

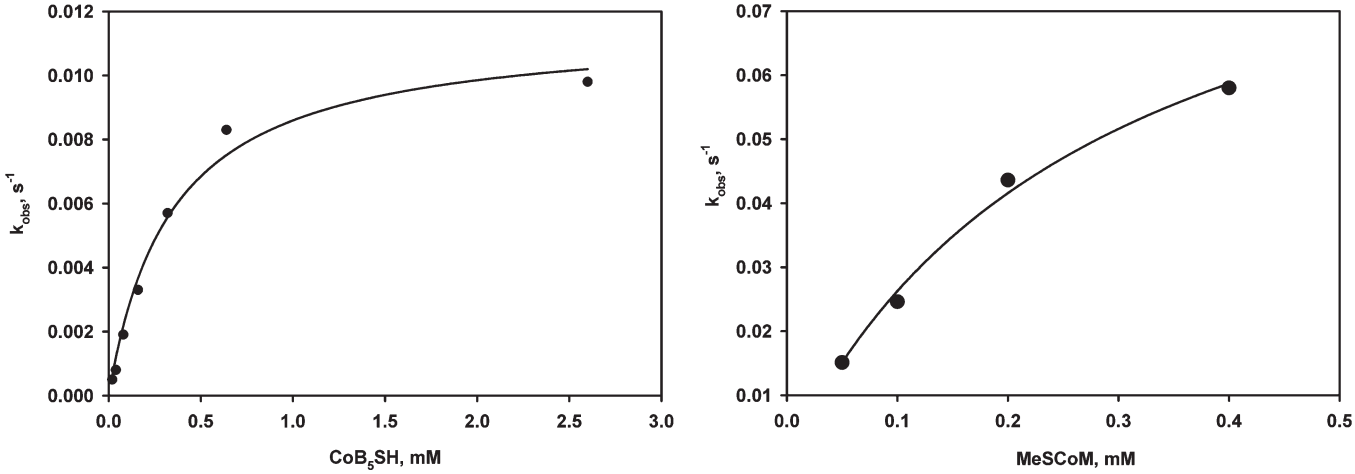

FIGURE 6: Dependence of k_{obs} for the reactions between MCR_{red1}, CoB_5SH, and MeSCoM. Left: MCR_{red1} (10 μM) was reacted with 1 mM MeSCoM and different concentrations of CoB_5SH. $k_{max} = 0.01 \pm 0.00\ s^{-1}$; $K_M = 0.34 \pm 0.06$ mM; $k_{max}/K_M = 35.2\ M^{-1}\ s^{-1}$. Right: MCR_{red1} (10 μM) was reacted with 200 μM CoB_5SH and different concentrations of Me-SCoM. $k_{max} = 0.10 \pm 0.05\ s^{-1}$; $K_M = 0.28 \pm 0.05$ mM; $k_{max}/K_M = 357\ M^{-1}\ s^{-1}$. The reactions were monitored at 385 and 420 nm. The data were fit with a two-parameter hyperbolic equation.

populations with the high affinity form being poised to react with the second substrate faster than the low affinity form.

When CoB_5SH is reacted with MCR_{red1} in the presence of methyl-SCoM, the rate constant for MCR_{red1} decay (0.002 s^{-1}) is similar to that of Ni(II)/Ni(III) formation (0.0016 s^{-1}), which is approximately 50−100 times lower than that observed with CoB_6SH as a substrate (0.092 s^{-1}) (Figure S3 in the Supporting Information). As with the reaction with CoB_6SH, the k_{obs} for MCR_{red1} decay is dependent on the concentrations of both CoB_5SH and methyl-SCoM (Figure 6) with second order rate constants of ~35 $M^{-1}\ s^{-1}$ (CoB_5SH dependence) and ~357 $M^{-1}\ s^{-1}$ (methyl-SCoM dependence). In fact, the k_{max}/K_M for methyl-SCoM is similar to the steady-state k_{cat}/K_M (methyl-SCoM) for methane formation (930 $M^{-1}\ s^{-1}$ at 20 °C), which supports our hypothesis that the chemistry and kinetics of the steps in methanogenesis preceding CoBSH binding are identical for CoBSH and CoB_5SH. On the other hand, the k_{max}/K_M for CoB_5SH (35 $M^{-1}\ s^{-1}$) is 50−100 times slower than the k_{cat}/K_M for CoBSH in methane formation ($2.2 \times 10^3\ M^{-1}\ s^{-1}$ at 20 °C) (*22*). The kinetic data of the methyl-SCoM/CoB_5SH reaction, therefore, support the proposal that CoBSH influences the first step in methanogenesis but is not directly involved in generating the first intermediate.

When MCR_{red1} is incubated with CoBSH and relatively longer CoBSH analogues, i.e., CoB_8SH or CoB_9SH in the presence of methyl-SCoM, no change in the UV−visible spectrum is observed (data not shown).

EPR Characterization of the Reaction of MCR_{red1} with Methyl-SCoM and CoB_6SH. Single turnover conditions were used to monitor by EPR the reaction of MCR_{red1} with CoB_6SH and methyl-SCoM. An organic radical (centered at approximately 3330 G) with a *g* value of 2.004 is observed (inset of Figure 7, solid line). Our data suggest that this radical forms with a rate constant (0.02 s^{-1}) that is similar to the k_{cat} for methane formation from methyl-SCoM and CoB_6SH and only 4-fold slower than the rate constant for MCR_{red1} decay (0.08 s^{-1}) (Figure 6). Thus, this radical appears to be an intermediate in the catalytic cycle. Under identical conditions, when CoB_5SH is substituted for CoB_6SH, MCR_{red1} decays 50-fold more slowly (0.002 s^{-1}) but the radical species is not observed (data not shown). If the rate of

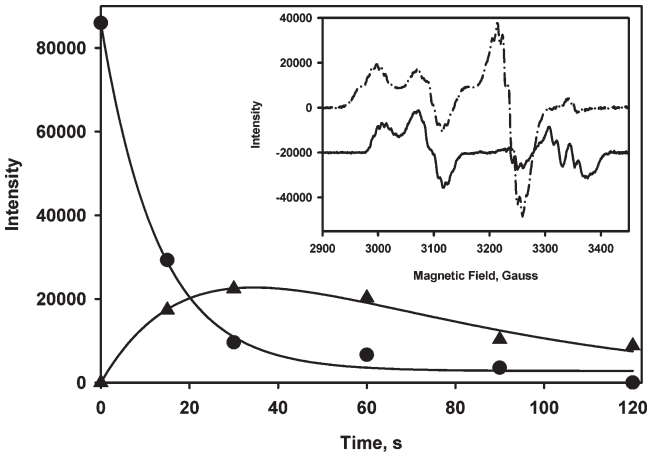

FIGURE 7: Organic radical generation from the reaction of MCR_{red1}, CoB_6SH, and methyl-SCoM. EPR samples were taken at various times, and the intensities of MCR_{red1} (●) and organic radical (▲) were measured, $k_{red1\text{-}decay} = 0.078\ s^{-1}$, $k_{radical\text{-}form} = 0.020\ s^{-1}$, and $k_{radical\text{-}decay} = 0.041\ s^{-1}$. Inset: EPR spectrum of starting MCR_{red1} (dashed−dotted line) and 30 s after the start of the reaction (solid line).

radical decay is similar to that seen with CoB_6SH ($0.041\ s^{-1}$), then it decays 25-fold faster than the rate constant of MCR_{red1} decay ($0.002\ s^{-1}$); therefore, it would not be able to accumulate to detectable levels when CoB_5SH is used as a substrate.

Isotopic Substitution and EPR Spectroscopic Experiments to Determine if the Organic Radical Species Derives from a Tyrosyl Radical. The $g = 2$ region of the radical spectrum (Figure 7 inset) reveals a partially resolved four-line pattern with a g value of 2.0035 and a peak-to-trough line width of ~25 G, which is typical of neutral tyrosine radicals (*40*), as observed in LipA (*41*), photosystem II (*42*), and ribonucleotide reductase (*43*). Furthermore, the crystal structure of Ni(II)-MCR reveals two tyrosines, Tyr α333 and Tyr β367, at the active site with their phenolate oxygens at 4.4 and 4.3 Å, respectively, from the nickel center. Therefore, it was hypothesized that the radical doublet EPR signal derives from one of these Tyr residues. Because the hyperfine structures of tyrosine radicals are sensitive to the orientation of the ring headgroup and to the β-hydrogen atoms relative to the protein backbone, isotopic labeling experiments were performed in order to identify the origin of the organic radical species.

In order to test the hypothesis that the radical intermediate detected by EPR and UV−visible spectroscopic studies derives from Tyr, perdeuterated ($^2H_6$) tyrosine was incorporated into the protein by growing cells with $^2H_6$-*p*-OH-phenylacetate, which is a precursor for the biosynthesis of tyrosines in methanogens (*35*). $^2H_6$-Tyr-labeled MCR_{red1} was reacted with methyl-SCoM in the presence of CoB_6SH. If the EPR spectrum is associated with one of the two Tyr residues located immediately above the Ni center at the active site of MCR, a significant change in the line shape is expected upon substitution of these $^1H_6$-Tyr residues with $^2H_6$-Tyr. If the spin is associated with a Tyr residue, the hyperfine couplings would be expected to narrow to a single line, as was observed with isotopic substitution experiments in the tyrosyl radical in photosystem II (*44*). As shown in Figure 8, there was no detectible difference between the radical doublet EPR spectra of the MCR samples prepared in media containing natural abundance versus ^{2}H-Tyr. The fact that these spectra exhibit the same line-width unambiguously rules out the hypothesis that the radical intermediate, which is generated from the reaction of

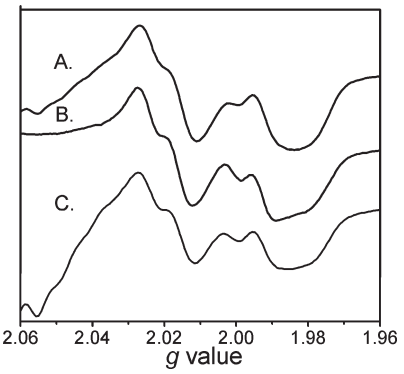

FIGURE 8: X-band EPR spectra of the radical in the endogeneous and [^{2}H-6] deutero tyrosine-substituted MCR. MCR_{red1} /^{2}H-Tyr MCR_{red1} (100 μM) was incubated with 1 mM methyl-SCoM and 300 μM CoB_6SH in 50 mM Tris pH 7.6 at 20 °C, and the samples were frozen away 30 s after the start of the reaction. (A) MCR_{red1} + methyl-SCoM + CoB_6SH in aqueous buffer and natural abundance Tyr, (B) same conditions as in part A in D_2O, (C) same conditions as in part A except using ^{2}H-Tyr MCR_{red1}.

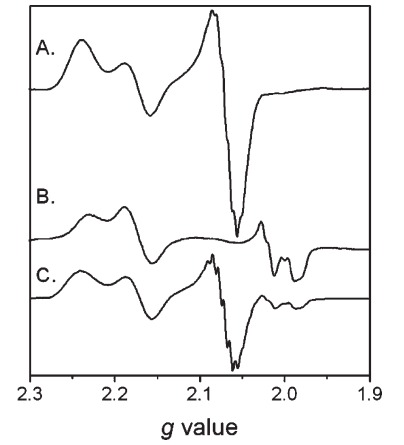

FIGURE 9: EPR spectra of 100 μM MCR_{red1} after reaction with (A) acetyl-tyrosine, (B) 1 mM methyl-SCoM in the presence of 300 μM CoB_6SH, and (C) acetyl-tyrosine followed by reaction with methyl-SCoM and CoB_6SH (as in spectrum B). EPR parameters: microwave frequency, 9.384 GHz; microwave power, 10.440 mW; modulation frequency, 100 kHz; modulation amplitude, 10 G; and temperature, 70 K.

MCR_{red1} with methyl-SCoM and CoB_6SH and exhibits the doublet EPR spectrum, is a tyrosyl radical.

Effect of Tyrosyl Acetylation. Even though the methyl-SCoM-generated radical does not derive from tyrosine, the tyrosyl residues appear to still play an important role in radical formation. Acetylation of tyrosyl residues in MCR_{red1} by treatment with *N*-acetylimidazole has no effect on the EPR spectrum of MCR_{red1}; however, Tyr acetylation blocks the formation of the methyl-SCoM-generated radical (Figure 9A). The amount of radical generated from the reaction of acetylated MCR_{red1} with methyl-SCoM and CoB_6SH is greatly decreased and a significant amount of MCR_{red1} remains (Figure 9C), as compared with the reaction of unlabeled MCR_{red1} with methyl-SCoM and CoB_6SH.

DISCUSSION

Two limiting mechanisms for MCR-catalyzed methane synthesis have been proposed (Figure 1). The major distinction between the two competing mechanisms lies in the proposed intermediate generated in the first step of catalysis: an organometallic

methyl-Ni(III) in Mechanism I or in Mechanism II, a methyl radical and a Ni(II)-SCoM species. Discrimination between these has not been possible because no intermediates in the MCR reaction with methyl-SCoM and CoBSH have been detected by transient kinetic (stopped-flow and rapid freeze quench EPR) methods. Furthermore, we have not observed any intermediate from the reaction of MCR_{red1} with methyl-SCoM alone, even under single turnover conditions, implying a role for CoBSH in promoting the first catalytic step (*30*).

An intermediate does not accumulate because its formation rate is too slow relative to the decay rate; thus, in order to trap a catalytic intermediate, we have used two strategies to modify the electronic and steric properties of the substrates to alter these formation and decay rates. Accelerating the first step in the MCR reaction was accomplished by reacting MCR_{red1} with a broad range of highly activated analogues of methyl-SCoM. Thus, the reaction of MCR_{red1} with haloalkanes (like methyl iodide), haloalkane sulfonates (e.g., bromopropane sulfonate, BPS), and haloalkanoates generates the corresponding alkyl-Ni(III) species at rates exceeding the rate of methane formation using natural substrates (*25*−*28*). The alkyl-Ni(III) products appear to be reasonable mechanism-based substrate analogues because they undergo protonolysis to generate the corresponding alkane (*26*, *28*) and thiolysis upon reaction with various thiolates, including HSCoM, to generate the active Ni(I)-MCR_{red1} state and the corresponding thioether products (i.e., methyl-SCoM when methyl-Ni(III) is reacted with HSCoM) (*27*).

Here, we describe a second strategy to generate intermediates in the MCR catalytic cycle, by reacting MCR_{red1} with the natural substrate methyl-SCoM and substrate analogues of CoBSH that are one and two methylene groups shorter than CoBSH (i.e., CoB_6SH, and CoB_5SH). The hypothesis is that the reactive thiolate of $HSCoB_6$ and $HSCoB_5$ would be located at least 2.0 Å further from the first intermediate (i.e., methyl-Ni or methyl radical) and would, thus, react slower than CoBSH, perhaps allowing us to trap and characterize the first intermediate in the reaction. The crystal structures of various CoBSH analogues at the substrate channel of MCR demonstrates the positioning of the terminal thiol groups, with CoB_6SH thiol located equidistant from Ni−F_{430} as CoBSH (8.7 Å), whereas CoB_5SH is about 9.3 Å away from the Ni center (*45*). Biochemical data have shown that CoB_6SH binds tightly to MCR (K_M = 0.1 μM (*10*)) and serves as a substrate with methyl-SCoM as the methyl donor, leading to a 100- (*10*) to 1000-fold (*30*) reduction (relative to CoBSH) in the k_{cat} for methane formation under steady-state conditions and a 440-fold reduction under single turnover conditions (*30*).

The results described here provide evidence that the reaction of MCR_{red1} with the natural substrate, methyl-SCoM, involves formation of an organometallic methyl-Ni(III) intermediate coupled to the decay of MCR_{red1}. This is the first time that an intermediate has been detected from the reaction of MCR with the natural substrate methyl-SCoM. Previous direct spectroscopic evidence for alkyl-Ni(III) species has been obtained only during reaction with activated haloalkanoates or haloalkane sulfonates (*24*−*27*). The ability to observe such an intermediate is based on the use of slow reacting substrate analogues of the second substrate (CoB_6SH and CoB_5SH) that contain only a slight structural perturbation. The appearance of a 495 nm shoulder, which is characteristic of the alkyl-Ni(III) state of MCR (*25*, *36*, *37*), provides strong evidence for the intermediacy of a methyl-Ni(III) species, which is a proposed intermediate in Mechanism I. This Ni(III) species decays rapidly with a half-life of ~4.0 s (k_{obs} = 0.17 s^{-1}) and did not accumulate sufficiently for further characterization.

The substrate-dependent amplitude changes (with either methyl-SCoM or CoB_6SH) for the biphasic kinetics accompanying decay of MCR_{red1} support the hypothesis that substrate binding triggers a conformational change that promotes binding of the second substrate. This hypothesis includes the existence of two populations of enzyme, "substrate-bound" and "substrate-free" forms that slowly interconvert, with the methyl-SCoM-bound state able to undergo a conformational change to rapidly react with CoBSH (or its analogue). Evidence for conformational changes in MCR upon substrate binding has also been reported, on the basis of the crystal structures of the inactive Ni(II) form of MCR (*17*) and recent EPR studies (*46*).

We also observed the formation of an organic radical intermediate that formed and decayed at rates (0.02−0.04 s^{-1}) that are too slow to allow it to be trapped. This organic radical intermediate was proposed to arise from Tyr β367, which is located 3.2 Å from the Ni-bound thiolate of SCoM (*23*), a distance that might allow it to act as a hydrogen atom donor to a methyl radical (forming methane) or to shuttle a hydrogen atom between CoBSH and SCoM. However, isotopic labeling experiments rule out the possibility that the observed radical is a tyrosyl radical. Other candidates for the identity of the radical include the α-thioglycine445 residue near the active site (12 Å from Ni), the thiolate group of CoMSH or $HSCoB_6$ (but the latter is ~9 Å from Ni), or the corphinoid ring of F_{430}.

Recent transient kinetic experiments of MCR_{red1} with BES and CoB_6SH identified three intermediates: an alkyl-Ni(III) species that forms as the active Ni(I)-MCR_{red1} state of the enzyme decays, a Ni(II)-MCR species, and an organic radical that is distinct from the radical described here from the reaction with methyl-SCoM but also was ruled out as a Tyr radical (*24*). The results described here are not inconsistent with the recently proposed hybrid mechanism; however, they are also consistent with Mechanism I in that the identified intermediates are alkyl-Ni(III) and an organic radical. The results described here with true substrates for the MCR reaction, methyl-SCoM and CoB_6SH (a slow substrate), provide further support for an organometallic-based methyl-Ni mechanism that is similar to Mechanism I but with slight modifications (Figure 10.)

In step 1 of the reaction, MCR_{red1} reacts with methyl-SCoM to form a methyl-Ni(III) intermediate (λ_{max} centered at 495 nm) and the $^{-}$SCoM anion, which undergoes protonation from CoBSH to form the $CoBS^{-}$ thiolate and HSCoM. In step 2, the transient methyl-Ni(III) intermediate undergoes metal-centered reduction coupled with electron transfer to form an EPR-silent methyl-Ni(II) species. Step 3 involves protonation of the Ni-bound methyl group to generate methane. Pulsed EPR and ^{19}F ENDOR experiments indicate that the proton derives from the thiol group of HSCoB (*4*, *47*); however, because CoBSH appears to be too distant to provide this proton directly, we speculate that HSCoM is the direct proton donor. Alternatively, a proton transfer network may be involved in generating HSCoM and we speculate that this could involve CoBSH, a solvent molecule that is observed in various structures of MCR containing CoBSH (*45*) and/or the Tyr residue(s) directly above the Ni center. Methane formation is coupled with generation of the new organic radical intermediate detected here and we speculate $CoMS^{\bullet}$ and $CoBS^{\bullet}$ as potential radical candidates. In step 4, we propose that an equilibration exists where the unidentified organic

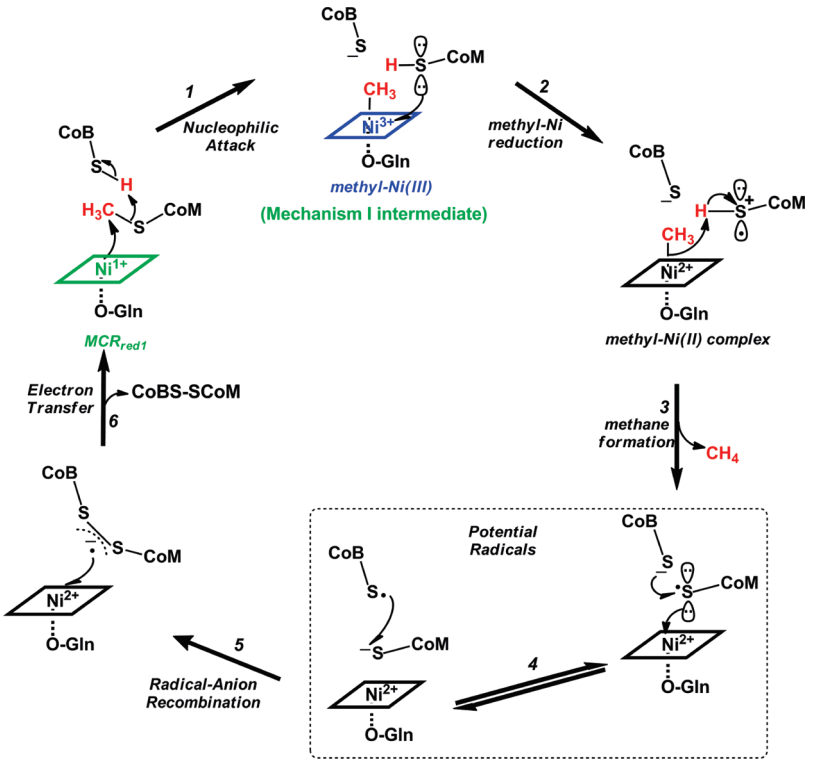

FIGURE 10: Revised mechanism for methane formation involving methyl-Ni (III) and an organic radical intermediate: (1) Nucleophilic attack of Ni(I) on the methyl group of methyl-SCoM to form methyl-Ni(III) and $^{-}$SCoB; (2) reduction of methyl-Ni(III) species to methyl-Ni(II); (3) proton transfer from HSCoM thiol to generate methane and a CoMS$^{\bullet}$ radical; (4) equilibration between the CoMS$^{\bullet}$ radical and CoBS^{-} to generate a CoBS$^{\bullet}$ thiyl radical; (5) condensation of the CoBS$^{\bullet}$ radical with the thiolate of $^{-}$SCoM to form a disulfide anion-radical intermediate; (6) electron transfer from disulfide anion radical to Ni(II) to complete the catalytic cycle by regenerating active Ni(I)-MCR$_{red1}$.

radical (e.g., CoMS$^{\bullet}$) abstracts a H-atom from CoBSH to form the CoBS$^{\bullet}$ radical and CoMS^{-}. The thiolate of CoMS might ligate to the nickel center to form a Ni(II)-thiolate complex. Thus, in this mechanism, there are two candidates for assignment of the g = 2.004 EPR signal: CoBS$^{\bullet}$ and CoMS$^{\bullet}$. Steps 5 and 6 are similar to those proposed in Mechanisms 1 and 2. Recombination of the CoBS$^{\bullet}$ radical with the thiolate of $^{-}$SCoM would form the heterodisulfide radical-anion, which would then be coupled to the final step of methanogenesis in which the active Ni(I)-MCR$_{red1}$ is regenerated *via* an one-electron reduction step. Thus, potential candidates for the identity of this new unidentified organic radical are CoBS$^{\bullet}$, $^{\bullet}$SCoM, and a nearby thioglycine residue.

CONCLUSIONS

With the the use of a CoBSH substrate analogie in which the heptanoyl moiety is replaced with a shorter hexanoyl carbon chain, the initial steps in the MCR reaction involving the natural substrate methyl-SCoM are sufficiently slowed to allow for the first time detection of the decay of the active Ni(I)-MCR$_{red1}$ state and formation of an alkyl-Ni(III) state. Furthermore, the methyl-Ni(III) decays to form a radical species. These results provide strong support for a reaction cycle resembling Mechanism I, which includes organometallic and radical intermediates. In future studies, it is important to identify the radical (by labeling the candidates, CoMSH, CoBSH) and to explore strategies, including the use of substrate analogues, that might allow the accumulation of sufficient amounts of the methyl-Ni(III) species for characterization by EPR and other spectroscopic studies.

SUPPORTING INFORMATION AVAILABLE

Biphasic kinetic data at low substrate concentration, dependence of rate constant (k_2) of the slow phase on substrate concentrations, amplitude change as a function of substrate concentrations for the reaction of MCR$_{red1}$ with methyl-SCoM and CoB$_6$SH monitored at 420 nm, and time-dependent UV−visible changes when MCR$_{red1}$ is reacted with CoB$_5$SH and methyl-SCoM. This material is available free of charge via the Internet at http://pubs.acs.org.

REFERENCES

1. Atreya, S. K., Mahaffy, P. R., and Wong, A. (2007) Methane and related trace species on Mars: Origin, loss, implications for life, and habitability. *Planet. Space Sci. 55*, 358–369.
2. Thauer, R. K. (1998) Biochemistry of methanogenesis: a tribute to Marjory Stephenson. *Microbiology 144*, 2377–2406.
3. Thauer, R. K., Kaster, A. K., Seedorf, H., Buckel, W., and Hedderich, R. (2008) Methanogenic archaea: ecologically relevant differences in energy conservation. *Nat. Rev. Microbiol. 6*, 579–591.
4. Ebner, S., Jaun, B., Goenrich, M., Thauer, R. K., and Harmer, J. (2009) Binding of Coenzyme B Induces a Major Conformational Change in the Active Site of Methyl-Coenzyme M Reductase. *J. Am. Chem. Soc. 132*, 567–575.
5. Kruger, M., Meyerdierks, A., Glockner, F. O., Amann, R., Widdel, F., Kube, M., Reinhardt, R., Kahnt, J., Bocher, R., Thauer, R. K., and Shima, S. (2003) A conspicuous nickel protein in microbial mats that oxidize methane anaerobically. *Nature 426*, 878–881.
6. Shima, S., and Thauer, R. K. (2005) Methyl-coenzyme M reductase and the anaerobic oxidation of methane in methanotrophic Archaea. *Curr. Opin. Microbiol. 8*, 643–648.
7. Thauer, R. K., and Shima, S. (2008) Methane as fuel for anaerobic microorganisms. *Ann. N.Y. Acad. Sci. 1125*, 158–170.
8. Scheller, S., Goenrich, M., Boecher, R., Thauer, R. K., and Jaun, B. (2010) The key nickel enzyme of methanogenesis catalyses the anaerobic oxidation of methane. *Nature 465*, 606–608.
9. DiMarco, A. A., Bobik, T. A., and Wolfe, R. S. (1990) Unusual coenzymes of methanogenesis. *Annu. Rev. Biochem. 59*, 355–394.
10. Ellermann, J., Hedderich, R., Böcher, R., and Thauer, R. K. (1988) The final step in methane formation. Investigations with highly purified methyl-CoM reductase (component C) from *Methanobacterium thermoautotrophicum* (strain Marburg). *Eur. J. Biochem. 172*, 669–677.

11. Ellefson, W. L., Whitman, W. B., and Wolfe, R. S. (1982) Nickel-containing factor F430: chromophore of the methylreductase of Methanobacterium. *Proc. Natl. Acad. Sci. U.S.A. 79*, 3707–3710.
12. Färber, G., Keller, W., Kratky, C., Jaun, B., Pfaltz, A., Spinner, C., Kobelt, A., and Eschenmoser, A. (1991) Coenzyme F430 from methanogenic bacteria: complete assignment of configuration based on an X-ray analysis of 12,13-diepi-F430 pentamethyl ester and on NMR spectroscopy. *Helv. Chim. Acta 74*, 697–716.
13. Goubeaud, M., Schreiner, G., and Thauer, R. K. (1997) Purified methyl-coenzyme-M reductase is activated when the enzyme-bound coenzyme F_{430} is reduced to the nickel(I) oxidation state by titanium-(III) citrate. *Eur. J. Biochem. 243*, 110–114.
14. Becker, D. F., and Ragsdale, S. W. (1998) Activation of methyl-SCoM reductase to high specific activity after treatment of whole cells with sodium sulfide. *Biochemistry 37*, 2639–2647.
15. Signor, L., Knuppe, C., Hug, R., Schweizer, B., Pfaltz, A., and Jaun, B. (2000) Methane formation by reaction of a methyl thioether with a photo-excited nickel thiolate-a process mimicking methanogenesis in archaea. *Chemistry 6*, 3508–3516.
16. Grabarse, W., Mahlert, F., Duin, E. C., Goubeaud, M., Shima, S., Thauer, R. K., Lamzin, V., and Ermler, U. (2001) On the mechanism of biological methane formation: structural evidence for conformational changes in methyl-coenzyme M reductase upon substrate binding. *J. Mol. Biol. 309*, 315–330.
17. Grabarse, W. G., Mahlert, F., Duin, E. C., Goubeaud, M., Shima, S., Thauer, R. K., Lamzin, V., and Ermler, U. (2001) On the mechanism of biological methane formation: Structural evidence for conformational changes in methyl-coenzyme M reductase upon substrate binding. *J. Mol. Biol. 309*, 315–330.
18. Piskorski, R., and Jaun, B. (2003) Direct determination of the number of electrons needed to reduce coenzyme F430 pentamethyl ester to the Ni(I) species exhibiting the electron paramagnetic resonance and ultraviolet-visible spectra characteristic for the MCR(red1) state of methyl-coenzyme M reductase. *J. Am. Chem. Soc. 125*, 13120–13125.
19. Jaun, B. Methane formation by methanogenic bacteria: redox chemistry of coenzyme F430 (1993) in Metal Ions in Biological Systems (Sigel, H., Sigel, A., Eds.) pp 287−337, Marcel Dekker, New York.
20. Pelmenschikov, V., Blomberg, M. R. A., Siegbahn, P. E. M., and Crabtree, R. H. (2002) A Mechanism from Quantum Chemical Studies for Methane Formation in Methanogenesis. *J. Am. Chem. Soc. 124*, 4039–4049.
21. Pelmenschikov, V., and Siegbahn, P. E. (2003) Catalysis by methyl-coenzyme M reductase: a theoretical study for heterodisulfide product formation. *J. Biol. Inorg. Chem. 8*, 653–662.
22. Chen, S. L., Pelmenschikov, V., Blomberg, M. R., and Siegbahn, P. E. (2009) Is there a Ni-methyl intermediate in the mechanism of methyl-coenzyme M reductase? *J. Am. Chem. Soc. 131*, 9912–9913.
23. Duin, E. C., and McKee, M. L. (2008) A New Mechanism for Methane Production from Methyl-Coenzyme M Reductase As Derived from Density Functional Calculations. *J. Phys. Chem. B 112*, 2466–2482.
24. Li, X., Telser, J., Kunz, R. C., Hoffman, B. M., Gerfen, G., and Ragsdale, S. W. (2010) Observation of organometallic and radical intermediates formed during the reaction of methyl-coenzyme M reductase with bromoethanesulfonate. *Biochemistry 49*, 6866–76.
25. Dey, M., Kunz, R. C., Lyons, D. M., and Ragsdale, S. W. (2007) Characterization of Alkyl-Nickel Adducts Generated by Reaction of Methyl-Coenzyme M Reductase with Brominated Acids. *Biochemistry 46*, 11969–11978.
26. Dey, M., Telser, J., Kunz, R. C., Lees, N. S., Ragsdale, S. W., and Hoffman, B. M. (2007) Biochemical and Spectroscopic Studies of the Electronic Structure and Reactivity of a Methyl-Ni Species Formed on Methyl-Coenzyme M Reductase. *J. Am. Chem. Soc. 129*, 11030–11032.
27. Kunz, R. C., Dey, M., and Ragsdale, S. W. (2008) Characterization of the Thioether Product Formed from the Thiolytic Cleavage of the Alkyl-Nickel Bond in Methyl-Coenzyme M Reductase. *Biochemistry 47*, 2661–2667.
28. Kunz, R. C., Horng, Y.-C., and Ragsdale, S. W. (2006) Spectroscopic and Kinetic Studies of the Reaction of Bromopropanesulfonate with Methyl-Coenzyme M Reductase. *J. Biol. Chem. 281*, 34663–34676.
29. Horng, Y. C., Becker, D. F., and Ragsdale, S. W. (2001) Mechanistic studies of methane biogenesis by methyl-coenzyme M reductase: evidence that coenzyme B participates in cleaving the C-S bond of methyl-coenzyme M. *Biochemistry 40*, 12875–12885.
30. Horng, Y.-C., Becker, D. F., and Ragsdale, S. W. (2001) Mechanistic Studies of Methane Biogenesis by Methyl-Coenzyme M Reductase: Evidence that Coenzyme B Participates in Cleaving the C-S Bond of Methyl-Coenzyme M. *Biochem. 40*, 12875–12885.
31. Ermler, U., Grabarse, W., Shima, S., Goubeaud, M., and Thauer, R. K. (1997) Crystal structure of methyl-Coenzyme M reductase: the key enzyme of biological methane formation. *Science 278*, 1457–1462.
32. Zehnder, A. J. B., and Wuhrmann, K. (1976) Titanium(III) citrate as a nontoxic oxidation-reduction buffering system for the culture of obligate anaerobes. *Science 194*, 1165–1166.
33. Gunsalus, R. P., Romesser, J. A., and Wolfe, R. S. (1978) Preparation of coenzyme M analogues and their activity in the methylcoenzyme M reductase system of *Methanobacterium thermoautotrophicum*. *Biochemistry 17*, 2374–2377.
34. Noll, K. M., Donnelly, M. I., and Wolfe, R. S. (1987) Synthesis of 7-mercaptoheptanoylthreonine phosphate and its activity in the methyl coenzyme M methylreductase system. *J. Biol. Chem. 262*, 513–515.
35. Porat, I., Sieprawska-Lupa, M., Teng, Q., Bohanon, F. J., White, R. H., and Whitman, W. B. (2006) Biochemical and genetic characterization of an early step in a novel pathway for the biosynthesis of aromatic amino acids and p-aminobenzoic acid in the archaeon Methanococcus maripaludis. *Mol. Microbiol. 62*, 1117–1131.
36. Mahlert, F., Bauer, C., Jaun, B., Thauer, R. K., and Duin, E. C. (2002) The nickel enzyme methyl-coenzyme M reductase from methanogenic archaea: In vitro induction of the nickel-based MCR-ox EPR signals from MCR-red2. *J. Biol. Inorg. Chem. 7*, 500–513.
37. Craft, J. L., Horng, Y.-C., Ragsdale, S. W., and Brunold, T. C. (2004) Nickel Oxidation States of F_{430} Cofactor in Methyl-Coenzyme M Reductase. *J. Am. Chem. Soc. 126*, 4068–4069.
38. Bonacker, L. G., Baudner, S., Mörschel, E., Böcher, R., and Thauer, R. K. (1993) Properties of the two isoenzymes of methyl-coenzyme M reductase in *Methanobacterium thermoautotrophicum*. *Eur. J. Biochem. 217*, 587–595.
39. Goenrich, M., Duin, E. C., Mahlert, F., and Thauer, R. K. (2005) Temperature dependence of methyl-coenzyme M reductase activity and of the formation of the methyl-coenzyme M reductase red2 state induced by coenzyme B. *J. Biol. Inorg. Chem. 10*, 333–342.
40. Hoganson, C. W., and Tommos, C. (2004) The function and characteristics of tyrosyl radical cofactors. *Biochim. Biophys. Acta 1655*, 116–122.
41. Wu, F., Katsir, L. J., Seavy, M., and Gaffney, B. J. (2003) Role of radical formation at tyrosine 193 in the allene oxide synthase domain of a lipoxygenase-AOS fusion protein from coral. *Biochemistry 42*, 6871–6880.
42. Un, S., Atta, M., Fontecave, M., and Rutherford, A. W. (1995) g-Values as a Probe of the Local Protein Environment: High-Field EPR of Tyrosyl Radicals in Ribonucleotide Reductase and Photosystem II. *J. Am. Chem. Soc. 117*, 10713–10719.
43. Hoganson, C., and Babcock, G. (1992) Protein-tyrosyl radical interactions in photosystem II studied by electron spin resonance and electron nuclear double resonance spectroscopy: comparison with ribonucleotide reductase and in vitro tyrosine. *Biochemistry 31*, 11874–11880.
44. Barry, B. A., el-Deeb, M. K., Sandusky, P. O., and Babcock, G. T. (1990) Tyrosine radicals in photosystem II and related model compounds. Characterization by isotopic labeling and EPR spectroscopy. *J. Biol. Chem. 265*, 20139–20143.
45. Cedervall, P. E., Dey, M., Pearson, A. R., Ragsdale, S. W., and Wilmot, C. M. (2010) Structural Insight into Methyl-Coenzyme M Reductase Chemistry using Coenzyme B Analogues. *Biochemistry 49*, 7683–7693.
46. Ebner, S., Jaun, B., Goenrich, M., Thauer, R. K., and Harmer, J. (2010) Binding of coenzyme B induces a major conformational change in the active site of methyl-coenzyme M reductase. *J. Am. Chem. Soc. 132*, 567–575.
47. Harmer, J., Finazzo, C., Piskorski, R., Ebner, S., Duin, E. C., Goenrich, M., Thauer, R. K., Reiher, M., Schweiger, A., Hinderberger, D., and Jaun, B. (2008) A nickel hydride complex in the active site of methyl-coenzyme m reductase: implications for the catalytic cycle. *J. Am. Chem. Soc. 130*, 10907–10920.